Dynamic phase diagram of soft nanocolloids†

Sudipta Gupta,[*a,b] Manuel Camargo,[c] Jörg Stellbrink,[*a] Jürgen Allgaier,[a] Aurel Radulescu,[d] Peter Lindner,[e] Emanuela Zaccarelli,[f] Christos N. Likos[g] and Dieter Richter[a]

We present a comprehensive experimental and theoretical study covering micro-, meso- and macroscopic length and time scales, which enables us to establish a generalized view in terms of structure–property relationship and equilibrium dynamics of soft colloids. We introduce a new, tunable block copolymer model system, which allows us to vary the aggregation number, and consequently its softness, by changing the solvophobic-to-solvophilic block ratio ($m : n$) over two orders of magnitude. Based on a simple and general coarse-grained model of the colloidal interaction potential, we verify the significance of interaction length σ_{int} governing both structural and dynamic properties. We put forward a quantitative comparison between theory and experiment without adjustable parameters, covering a broad range of experimental polymer volume fractions ($0.001 \leq \phi \leq 0.5$) and regimes from ultra-soft star-like to hard sphere-like particles, that finally results in the dynamic phase diagram of soft colloids. In particular, we find throughout the concentration domain a strong correlation between mesoscopic diffusion and macroscopic viscosity, irrespective of softness, manifested in data collapse on master curves using the interaction length σ_{int} as the only relevant parameter. A clear reentrance in the glass transition at high aggregation numbers is found, recovering the predicted hard-sphere (HS) value in the hard-sphere like limit. Finally, the excellent agreement between our new experimental systems with different but already established model systems shows the relevance of block copolymer micelles as a versatile realization of soft colloids and the general validity of a coarse-grained approach for the description of the structure and dynamics of soft colloids.

1. Introduction

Recent studies on soft matter include a large variety of complex fluids like synthetic polymers, biological macromolecules, colloids, amphiphilic systems, membranes as well as liquid crystals. A currently active field of research is focused on the special class of soft colloids, *i.e.* elastic and deformable colloidal particles, which display a dual character between polymers and hard spheres.[1,2] Examples of such soft colloids are vesicles, dendrimers,[3] microgels,[4,5] polymer-grafted nanoparticles,[6] block copolymer micelles[7–10] and star polymers.[11–13] Due to their hybrid nature, soft colloids macroscopically show interesting structural and dynamic properties resulting from their unique microscopic structure.

In particular, soft colloids featuring a star-like architecture constitute a natural bridge between polymers and colloids.[14] In such a case, an important microscopic structural parameter determining the softness of the macromolecular aggregate is the number of polymer chains that are anchored to the common center, *i.e.*, the functionality (f) for star polymers or the aggregation number (N_{agg}) for block copolymer micelles. For the latter system, easy and elegant ways to tailor the softness of micelles, *i.e.* their morphology and/or their aggregation number, can be achieved by varying the solvophobic-to-solvophilic block ratio‡ ($m : n$), the block length (M_w) and/or the interfacial tension, γ_{int}, between the solvophobic core and a selective solvent.[10,15] Fig. 1 shows a schematic representation of the morphological evolution of block copolymer micelles,

*a*JCNS-1 and ICS-1, Forschungszentrum Jülich, Leo-Brandt-Straße, 52425 Jülich, Germany. E-mail: s.gupta@fz-juelich.de, j.stellbrink@fz-juelich.de
*b*JCNS-SNS, Oak Ridge National Laboratory (ORNL), Bethel Valley Road, TN-37831 Oak Ridge, USA
*c*Centro de Investigaciones en Ciencias Básicas y Aplicadas, Universidad Antonio Nariño, Km 18 via Cali-Jamundí, 760030 Santiago de Cali, Colombia
*d*JCNS-FRM II, Forschungszentrum Garching, Lichtenbergstraße 1, 85747 Garching, Germany
*e*Institute Laue-Langevin, 6, rue Jules Horowitz, 38042 Grenoble CEDEX 9, France
*f*CNR-ISC and Dipartimento di Fisica, Universitá di Roma La Sapienza Piazzale A. Moro 2, I-00185 Roma, Italy
*g*Faculty of Physics, University of Vienna, Boltzmanngasse 5, A-1090 Vienna, Austria
† Electronic supplementary information (ESI) available: SANS, DLS and Rheology data modeling. See DOI: 10.1039/C5NR03702F

‡ It is to be noted that the block ratios $m : n$ are calculated in terms of repetitive units, not in terms of molecular weight M_w (see Table 1)
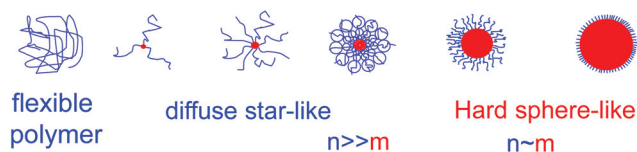
Fig. 1 Schematic representation of morphological evolution of star-like block copolymer micelles in selective solvent, from polymer-like Gaussian coil (N_{agg} = 1, 2) to hard sphere-like colloids ($N_{agg} \rightarrow \infty$). The numbers m and n denote the number of repeat units for the solvophobic (red) and the solvophilic (blue) blocks, respectively.

from polymer-like Gaussian coils (N_{agg} = 1 or 2) to colloid-like hard spheres ($N_{agg} \rightarrow \infty$), as the block ratio $m : n$ is changed.

From the theoretical point of view, the study of the macroscopic properties of suspensions of soft particles can be facilitated by appropriately coarse-graining their inherent complex intramolecular degrees of freedom, and subsequently a description of the system in terms of an effective pair potential can be provided by using standard statistical mechanics tools.[14,16,17] The most striking feature of such effective potential is that of presenting an ultrasoft logarithmic repulsion when two star-like particles significantly overlap in good solvent conditions (see eqn (1) below). This kind of repulsion is fundamentally different from that of other colloidal particles for which the interaction features an inverse power-law dependence for small distance,[18,19] and it is responsible for the theoretically predicted anomalous structural behavior[14,17] and for the formation of several equilibrium crystal structures at higher packing fractions of the constituent mesoscopic entities.[20–24]

The equilibrium phase diagram of suspensions of star-like soft colloids has been experimentally studied by Laurati et al.,[10,25] who employed kinetically frozen micelles formed by the amphiphilic block copolymer poly(ethylenepropylene)–poly(ethyleneoxide), PEP–PEO. In that work, the aggregation number was tuned by varying the solvent composition, i.e. by changing γ_{int}. These authors investigated the structure–property-relationship (SPR) starting from the aforementioned coarse-grained model and were able to confirm quantitatively theoretical predictions concerning the equilibrium phase diagram in the plane spanned by the concentration and the aggregation number by means of small angle neutron scattering experiments (SANS).[10,25] Later, Lonetti et al. extended this approach to the study of binary mixtures of ultra-soft colloids and linear polymers.[26,27] However, detailed investigation of the solid-like crystalline and glassy phases is still lacking. Moreover, some new questions arose with respect to the formation of non-equilibrium gel or glass phases and, in particular, on non-equilibrium flow properties in the ultrasoft, star-like regime.[13,28] Recently, using rheology as the primary technique, a dynamic phase diagram in temperature-shear rate space was reported for surfactant molecules.[29,30] There a temperature dependent transition from planar lamellae to multilamellar vesicles (MLVs) was observed.

Although there are several studies on the dynamics of soft colloids,[31,32] a full quantitative comparison between experiment and theory relating microscopic structure and meso- and macroscopic dynamics is still missing. Ideally, such a comparison should cover the complete range of softness (from ultra-soft star-like to hard sphere-like) using the same precisely defined model system to avoid any ambiguity from mapping one experimental system to the other. In the present work we aim at a generalized approach using a new soft colloidal model system based on poly(butylene oxide)–poly(ethylene oxide) block copolymer micelles, which enables us to cover a broad range of aggregation numbers and consequently softness. In particular, we performed a comprehensive experimental and theoretical study covering micro-, meso- and macroscopic length and time scales by applying precise dynamic techniques including dynamic light scattering (DLS) and rheology measurements. The materials and the systems are described in Section 2, together with the theoretical and experimental techniques applied to the analysis of the results. The latter are presented in Section 3 and the obtained dynamic data are interpreted in terms of the static structural properties derived by complimentary SANS experiments and liquid state theory. In particular, the location of the glass or gel line in the dynamic phase diagram and the validity of the Stokes-Einstein relation is investigated. An extensive discussion is presented in Section 4, whereas in Section 5 we summarize and draw our conclusions.

2.   Materials and methods

2.1   Sample description and experimental techniques

We employed aqueous solutions of the block copolymer poly(butylene oxide)–poly(ethylene oxide), PBO–PEO, which was recently synthesized by anionic polymerization.[34] PBO is slightly less hydrophobic[34–36] ($\gamma_{int,PBO}$ = 36 mN m^{-1}) with respect to water than the previously used poly(ethylene–propylene) PEP ($\gamma_{int,PEO}$ = 46 mN m^{-1}),[37] a property which allows an even more precise fine-tuning of the micellization behavior. For contrast variation SANS experiments, we used both protonated (hPEO) and deuterated (dPEO) PEO blocks, whereas the PBO block was always protonated (hPBO). This new synthesis technique allows us to achieve also high molecular weights with small polydispersity for the PBO block, which would otherwise crucially hamper the aggregation behavior. Therefore we can systematically vary the PBO : PEO block ratio over two orders of magnitude, $1 : 1 \lesssim m : n \lesssim 1 : 100$ (see Table 1), and thereby we approach gradually from the ultrasoft star-like to the hard sphere-like regime. In this way, we quantitatively investigate the phase diagram using the same well-defined model system and covering the full range of colloid "softness".

For highly asymmetric block ratios we observe a rather high critical micelle concentration (CMC), $\phi_{CMC} \approx 0.5\%$, which causes the presence of non-aggregated block copolymers (unimers) in the suspension. However, the resulting depletion interactions due to the presence of unimers are negligible at

Table 1 Molecular weight (M_w) characterization: the PBO : PEO block ratio ($m : n$) was calculated in terms of repetitive units; M_w/M_n is the poly-dispersity index[33] determined by ^{1}H-NMR and SEC. The aggregation number N_{agg} was obtained from SANS measurements

Diblock copolymer	$M_{w,PBO}$ (g mol^{-1})	$M_{w,PEO}$ (g mol^{-1})	Block ratio ($m : n$)	M_w/M_n	N_{agg}
hPBO0.9-hPEO50	900	58 700	1 : 107	1.02	25 ± 5
hPBO0.6-hPEO50	680	42 000	1 : 101	1.11	30 ± 4
hPBO1-hPEO50	960	52 400	1 : 89	1.08	50 ± 5
hPBO0.9-dPEO50	900	50 900	1 : 85	1.02	39 ± 5
hPBO2.5-dPEO50	2570	63 900	1 : 37	1.05	176 ± 10
hPBO2.5-hPEO50	2570	53 300	1 : 34	1.05	104 ± 5
hPBO10-dPEO50	10 500	52 500	1 : 8	1.02	500 ± 10
hPBO5-hPEO5	4920	5412	1 : 2	1.06	920 ± 20

such small unimer concentrations,[26,38,39] as shown by liquid state theory described in subsection 2.2.

All solutions were prepared by weight using an analytical balance and the corresponding experimental volume fractions ϕ were calculated assuming ideal mixing. We covered a broad range of block copolymer volume fractions $0.001 \leq \phi \leq 0.5$, which corresponds in terms of the overlap volume fraction of the block copolymers, $\phi_p^* = (V_w/N_A)/(4\pi R_{g,p}^3/3)$, to $0.001 \leq \phi/\phi_p^* \leq 53$, or in terms of the overlap volume fraction of the micelles, $\phi_m^* = N_{agg}(V_w/N_A)/(4\pi R_m^3/3)$, to $0.01 \leq \phi/\phi_m^* \leq 10$. Here, V_w is the polymer molecular volume, N_A is Avogadro's number, $R_{g,p}$ and R_m the radius of gyration of block copolymer (unimer) and micellar radius respectively, as determined by SANS experiments.

SANS experiments were carried out at different SANS diffractometers: KWS-1 and KWS-2 at Jülich Centre for Neutron Science (JCNS)/Heinz-Maier-Leibnitz-Zentrum (MLZ) in Garching (Germany), and D11 at Institute Laue Langevin (ILL) in Grenoble (France). The probed range was $0.001 \leq Q \leq 0.5$ Å^{-1}, with scattering vector $Q = (4\pi/\lambda)\sin(\theta/2)$, neutron wavelength λ and scattering angle θ. Data were reduced following standard procedures to correct for contributions resulting from empty cell, solvent and incoherent scattering and finally normalized by a water or plexi-glass standard using QtiKWS[40] and LAMP.[41]

To investigate the visco-elastic flow behaviour and influence of softness with varying asymmetry, size, aggregation number and volume fraction, we performed rheological experiments using both stress- (AR-G2) and strain-controlled (ARES-G2) rheometers from Rheometric Scientific Company. We used cone-plate geometry made of stainless steel of cone diameter 20–50 mm at a cone angle 0.01–0.04 radian, depending on the concentration of the samples. Temperature control of 20 ± 0.01 °C was set *via* a Peltier plate and was cooled by a circulating fluid bath thermostat (Julabo, Germany). From rheology we measured the change in viscosity as a function of shear rate by direct flow curves, covering a shear rate range, $10^{-5} \leq \dot{\gamma} \leq 3 \times 10^3$ s^{-1}. By repeating each measurement we have checked the data reproducibility. To ensure steady state of the sheared sample we followed a strict protocol as described by Petekidis *et al.*[42] We measured each data point (shear rate) at 300 s intervals along with increase in measurement time as the shear

rate, $\dot{\gamma}$ decreases. We followed a 10 s pre-shear protocol, followed by a 10 s measurement, for all $\dot{\gamma} > 1$ s^{-1}. A pre-shear for 100 s, followed by a 100 s measurement time for $10^{-2} \leq \dot{\gamma} \leq 1$ s^{-1}. Finally a pre-shear of 1000 s, with a 1000 s measurement time for all $\dot{\gamma} < 10^{-2}$ s^{-1}. To determine the solid-like behavior we performed oscillatory frequency sweep experiments over a frequency range, $10^{-2} \leq \omega \leq 10^2$ rad s^{-1} with strain amplitude of 1%. We followed a pre-shear protocol of 200 s interval of oscillatory shearing at $\omega = 1$ rad s^{-1} with strain amplitude of 100%, which placed the system in an initially homogeneous reproducible state. Each data point was measured for 10 s for $\omega > 1$ rad s^{-1}, and 100 s for $\omega \leq 1$ rad s^{-1}.[12] To avoid sample evaporation for long measurement time we sealed the sample with a layer of Dodecane around the cone and plate of the rheometer.

Corresponding SLS/DLS measurements were performed on a standard light scattering setup with ALV-125 compact goniometer and ALV5000E correlator covering a range of scattering angles $20° \leq \theta \leq 150°$ and corresponding Q-range $4 \times 10^{-4} \leq Q \leq 3 \times 10^{-3}$ Å^{-1}. Two different lasers were used (Ar$^+$ with $\lambda = 5145$ Å and He–Ne with $\lambda = 6328$ Å) depending on the scattering intensity of the sample. It is to be noted that for all experiments D$_2$O was used as the solvent, with viscosity $\eta_{solv} \approx 1.221$ mPa s at 20 °C. For SANS analysis the corresponding scattering length densities $\rho_{D_2O} = 6.36 \times 10^{10}$ cm^{-2}, $\rho_{hPBO} = 2.00 \times 10^9$ cm^{-2}, $\rho_{hPEO} = 6.79 \times 10^9$ cm^{-2}, and $\rho_{dPEO} = 7.52 \times 10^{10}$ cm^{-2} were used.

2.2 Theory and modeling

As mentioned above, our theoretical approach is based on a coarse-grained method introduced to study star polymers in good solvent conditions, for which the excluded volume interaction between monomers forming the stars is the only interaction taken into account.[14,17] Though at first sight it would appear inaccurate to ignore dispersion interactions between the sovophobic cores of the micelles, it turns out that this is not the case. In the range of very long chains, $m \ll n$, the core is small in size and thus the van der Waals attractions are overwhelmed by the steric repulsions of the chains. In the limit of almost symmetric blocks, and in particular for the $m : n = 1 : 2$ case (last entry in Table 1), the aggregation number is very

high, so that the chains provide, again, a sufficiently strong steric stabilization and the system behaves, effectively, like a hard sphere. We emphasize, however, anticipating scattering results to follow, that this system is different from the rest in Table 1, in the sense that it cannot be described as a soft, star-like object.

To provide a theoretical model for the effective interactions between our micelles, we simplify them as star polymers and considered the center of the star polymer as effective coordinate. The coarse-grained, star–star interaction $U(r)$ at center-to-center separation r displays a logarithmic dependence at short distances between the centers and an exponentially Yukawa decay at large ones. Since the potential diverges logarithmically as $r \to 0$, star polymers can be viewed as ultrasoft colloidal particles, which can interpenetrate and overlap with one another to a large extent. The star–star effective interaction is given by:[17]

$$\beta U(r) = \Theta \begin{cases} -\ln\left(\frac{r}{\sigma_{int}}\right) + \frac{1}{1+\sqrt{N_{agg}/2}} & r \leq \sigma_{int} \\ \frac{1}{1+\sqrt{N_{agg}/2}}\left(\frac{\sigma_{int}}{r}\right)\exp\left[-\frac{\sqrt{N_{agg}}}{2}\left(\frac{r-\sigma_{int}}{\sigma_{int}}\right)\right] & r > \sigma_{int} \end{cases} \quad (1)$$

where $\Theta = (5/18)N_{agg}^{3/2}$ and $\beta = (k_B T)^{-1}$, with k_B the Boltzmann constant and T the absolute temperature. The only characteristic length scale is the interaction length σ_{int}, which is defined according to the Daoud–Cotton model[43,44] as twice the distance from the star center to the center of the outermost blob. A generalized form of this effective potential was proposed for star-chain[45,46] and chain–chain[47,48] binary mixtures,§ opening the way for exploring experimentally the features of anomalous depletion predicted by theory,[26] and also on the recent findings on soft colloid-polymer mixtures.[27] Once the pair interaction potential is defined, the structural information of the system, namely the theoretical (micelle–micelle) static structure factor $S(Q)$, can be gained by numerically solving the Ornstein–Zernike (OZ) equation for different theoretical volume fraction $\phi_{TH} = (\pi/6)N_z\sigma_{int}^3$, where N_z is the number density of micelles. The OZ equation was iteratively solved with the help of the hypernetted chain closure (OZ-HNC),[19] which has been shown to be very reliable for soft potentials both in pure systems as in mixtures.[26,27,45,47,48]

On the other hand, for SANS the total scattering intensity $I(Q)$ is given by the product of the micellar form factor $P(Q)$, which is proportional to the scattering of a single micelle, and the structure factor $S(Q)$, which comprises the interaction effects. For a monodisperse collection of spherically symmetric particles it can be written as[49]

$$I(Q) \propto N_z P(Q) S(Q). \quad (2)$$

For dilute concentration $S(Q) = 1$ so that the scattering contribution for $P(Q)$ is experimentally determined by fitting a core–shell model following Svaneborg and Pedersen.[50,51] Here,

§ From now on, as chain we refer to a linear polymer having the same chemical nature than the star polymer.

the overall scattering intensity of a single block copolymer micelle is given by:[15,39,51,52]

$$I_{cs}(Q) \propto I_{core}(Q) + I_{corona}^b(Q) + I_{inter}(Q) + I_{blob}(Q), \quad (3)$$

being the details of the proportionality constant explained in the ESI.† Each micelle was assummed to feature a homogeneous spherical core and a diffuse shell (corona), the latter following a star-like density profile with $\phi_{star}(r) \propto r^{-4/3}$ in accordance with the Daoud–Cotton scaling model.[43,44] To allow a smooth density decay at the micellar surface, the radial decay is weighted by a cutoff Fermi function. Thereby the star-like density profile of a micelle is modeled by:[15,25,53]

$$\varphi_{star}(r) \propto r^{-4/3}\left(1 + \exp\left[\frac{(r-R_m)}{s_s R_m}\right]\right)^{-1}, \quad (4)$$

where R_m is the micellar radius, which can be defined as the cutoff length of the Fermi function, and s_s is a dimensionless smearing parameter.

The first and second terms, $I_{core}(Q)$ and $I_{corona}^b(Q)$ in eqn (3) corresponds to the scattering contribution from the micellar core and corona respectively. The third contribution $I_{inter}(Q)$ comes from the interference term between the core and the corona.[39,51,52] Blob scattering in the corona, expressed in the last term $I_{blob}(Q)$, captures the contributions of short-range density fluctuation correlations due to chain–chain interactions. This term plays an important role when the corona interior is sufficiently dense, so that it behaves as a semidilute polymer solution whose concentration lies above the overlap value of the linear chains, forming thereby a transient network of intra-micellar blobs. Using a discrete model with n sites per chain, the scattering from a semidilute solution follows the predictions based on the polymer reference interaction site model (PRISM) theory,[54] and the random phase approximation (RPA)[55] for polymer solution and melts. Following Svaneborg and Pedersen,[50,51] the blob scattering from swollen corona chains was thus modeled as:

$$I_{blob}(Q) \propto \left(\frac{P_p(Q)}{1 + \hat{\nu}P_p(Q)}\right) \quad (5)$$

$\hat{\nu}$ is an effective virial type excluded volume parameter that scales with the effective concentration of the corona chains, and $P_p(Q)$ is the modeled Beaucage form factor of free chains.[56,57] For details of quantitative data modeling of the macroscopic scattering cross section $(d\Sigma/d\Omega)(Q)$ in absolute units $[cm^{-1}]$, see ESI.† The various parameters characterizing the micelles of our work are summarized in Table 2.

For the most asymmetric block ratios showing a finite CMC, i.e., $m:n = 1:85$, $1:89$, $1:101$, and $1:107$, the non-aggregated block copolymers (unimers) were independently characterized at very dilute volume fractions well below the CMC where no micelles yet exist. We employed also here the Beaucage form factor to model scattering from these unimers. At volume fractions above CMC, the Beaucage term was added to the micellar form factor but with fixed parameters describing the unimers from the dilute regime.

Table 2 Molecular characteristics of the micelles built by the block copolymers shown at the left column, as in Table 1. Shown are the radius of gyration R_g from SANS Guinier analysis and the hydrodynamic radius R_h from DLS, the interaction length σ_{int} from $S(Q)$ analysis as entering in eqn (1), as well as the micellar radius R_m and the smearing parameter s_s from SANS $P(Q)$ analysis as appearing in eqn (4)

Micellar system ($m:n$)	R_g (nm)	R_h (nm)	σ_{int} (nm)	R_m (nm)	s_s
hPBO0.9-hPEO50 (1 : 107)	15.3 ± 0.5	49.7 ± 3	36.9	25.0 ± 0.8	0.10
hPBO0.6-hPEO50 (1 : 101)	14.5 ± 0.2	42.9 ± 2	31.7	21.3 ± 0.8	0.10
hPBO1-hPEO50 (1 : 89)	15.3 ± 0.5	36.1 ± 4	30.1	25.7 ± 1.0	0.10
hPBO0.9-dPEO50 (1 : 85)	15.0 ± 0.3	38.3 ± 3	31.3	25.7 ± 1.0	0.10
hPBO2.5-dPEO50 (1 : 37)	33.0 ± 0.2	50.2 ± 1	47.2[a]	46.7 ± 2.0	0.11
hPBO2.5-hPEO50 (1 : 34)	31.0 ± 0.5	42.6 ± 2	42.4	45.4 ± 0.4	0.10
hPBO10-dPEO50 (1 : 8)	43.5 ± 0.8	72.7 ± 2	64.2[a]	61.6 ± 1.0	0.10
hPBO5-hPEO5 (1 : 2)	14.5 ± 0.5	—[b]	38.6[c]	19.3 ± 1.0	0.10

[a] Refinement by SANS iterations. [b] DLS not applicable due to turbid sample. [c] Hard-sphere like interaction length $2R_m$.

3. Results

3.1 Architecture of individual soft colloids

Full contrast form factors obtained by SANS in the dilute block copolymer regime ($\phi < 0.01$) are illustrated in Fig. 2 for varying block-ratio, and compared to the core–shell model for $I_{cs}(Q)$ given by eqn (3). From the data-analysis procedure it was observed that the form factor for the most symmetric block-ratio, i.e. $m:n = 1:2$, is better described by a compact homogeneous core–shell model with a constant density profile $\phi(r) \sim r^0$ for both core and corona, which elucidates the fact that micelles having this block-ratio resembles more closely to a hard sphere-like system. On the other hand, systems with asymmetries 1 : 8 or more are clearly star-like. Interestingly, it should be noted from Table 2 that with decrease in block ratio the relative size, R_h, with respect to the interaction length, σ_{int}, decreases, except for 1 : 8. It highlights the importance of swollen micellar morphology of $R_h = 72.7$ nm (dilute regime) for 1 : 8 block ratio that shrinks drastically, yielding an interaction length of 64.2 nm on approaching the overlap concentration, ϕ^*. The difference in R_h from DLS with respect to the corresponding R_m from SANS is attributed to the fact that we

were able to measure very low concentration ($\phi \simeq 5 \times 10^{-4}$) from DLS. That was not possible due to low scattering intensity from SANS ($\phi \geq 10^{-3}$).

As explained above, for highly asymmetric block-ratio (1 : 89 and 1 : 101 in Fig. 2), the presence of unimers leads to modeling the SANS scattering intensity with a form factor, which results from the superposition of unimer chains, $P_p(Q)$, and micelles, $I_{cs}(Q)$, with relative concentrations given by $\phi_{CMC} \simeq 5 \times 10^{-3}$. The coexistence of the unimers and an estimation of ϕ_{CMC} has been verified by complimentary dynamic light scattering (DLS) experiments.[39] This illustrates the fact that, for the block-ratios 1 : 89, 1 : 101 and 1 : 107, the suspensions resemble more closely to binary, ultrasoft mixtures,[26,27] with a chain-to-micelle size ratio about 0.6 for $N_{agg} = 30$. We concluded that with increase in the asymmetric nature of the block ratio, at first there is formation of micelles for the symmetric and intermediate block-ratios 1 : 2, 1 : 8 and 1 : 34, followed by the co-existence of micelles and unimers, with varying concentration for the highly asymmetric block-ratio 1 : 89, 1 : 101 and 1 : 107. It also leads to increase in softness, apart from influencing the micellar architecture, from hard-sphere like regime to ultra soft star-like or linear polymeric regime. This is represented schematically in Fig. 2, with the arrow pointing the direction of increasing asymmetry and hence softness. From the form factor analysis in dilute solution we independently obtain the important parameters like the aggregation number N_{agg} (Table 1) and the micellar size R_m, needed for the following structure factor $S(Q)$ analysis at higher volume fractions.

3.2 Interactions of soft colloids

To reconcile experimental information with the coarse-graining model, the interaction length σ_{int} defining the effective potential (see eqn (1)) was obtained by an iterative procedure.[27,37,45,47] We use $\sigma_{int} \approx (4/3)\bar{R}$ as a zero order approximation with $\bar{R}$ the mean micellar radius as obtained from SANS (micellar radius R_m) and DLS (hydrodynamic radius R_h), respectively. This starting value for σ_{int} together with the independently known micellar number density N_z were taken for calculating the (theoretical) volume fraction ϕ_{TH} as input for the OZ-HNC calculation of the structure factor $S(Q)$, see also
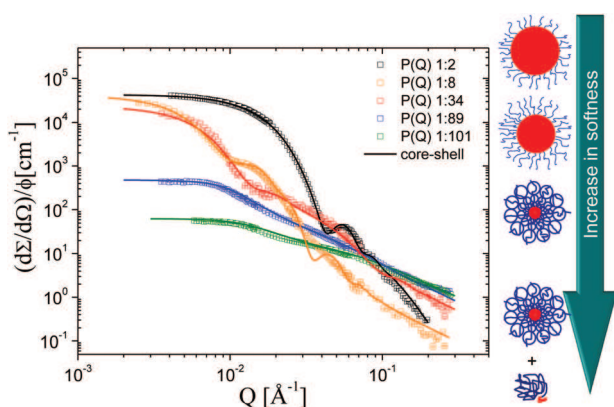

Fig. 2 Full contrast SANS micellar form factor at $\phi < 0.01$ for varying block-ratio. The continuous lines are fits to the core–shell model, eqn. (2) and (3), as explained in the main text. Side sketches: schematic representation of the micelles.
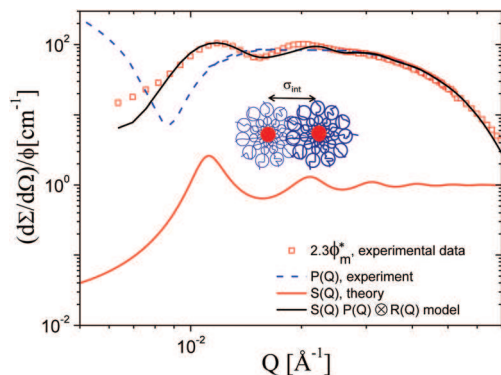
Fig. 3 Experimental normalized intensity $(d\Sigma/d\Omega)/\phi$ for $N_{agg} = 176$, $\phi/\phi_m^* = 2.3$ and asymmetry ratio $m : n = 1 : 37$, compared to the theoretical result, together with the separate contributions from the form factor, $P(Q)$, and the structure factor $S(Q)$. Here, both $P(Q)$ and σ_{int} have been modified according to shrinking as $\sim(\phi/\phi_m^*)^{-1/8}$ as the micelles exceed their overlap concentration, $\phi > \phi_m^*$.[43,59] Inset schematic illustration of overlapping micelles and their interaction length.

ref. 27. The SANS $I(Q)$ modeling was carried out by convoluting the product of pre-determined experimental form factor and theoretical structure factor with the instrumental resolution $R(Q)$,[58] i.e., $I(Q) \propto P(Q)S(Q) \otimes R(Q)$, without performing any fitting procedure.

The interaction length σ_{int} was confirmed for each block ratio (Table 2) from structure factor analysis for $\phi < \phi_m^*$, where it does not depend on micelle concentration. Its precise value was refined in several iterations following previous work[10,25,37] for two aggregation numbers 500 and 176 in partial core-contrast condition, by rescaling within experimental errors. For $N_{agg} = 500$ we covered a concentration range from $\phi/\phi_m^* = 0.7$ to 5 and for $N_{agg} = 176$ we covered $\phi/\phi_m^* = 1.3$ to 7.5. As a representative example in Fig. 3 the theoretical $Q\sigma_{int}$ abscissa is plotted to the experimental Q-range. Here the partial core-contrast SANS $I(Q)$ for $m : n = 1 : 37$ and $\phi/\phi_m^* = 2.3$ is illustrated in the open symbols for the forward scattering. The curves for $S(Q)$ calculated for $N_{agg} = 176$ and the corresponding $\phi_{TH} = 0.162$, $P(Q)$ from SANS and $P(Q)S(Q) \otimes R(Q)$ are also displayed in Fig. 3.

Since we are well above the overlap volume fraction, it is to be noted that the form factor $P(Q)$ has been modified taking into consideration the shrinkage of the micelle due to increasing osmotic pressure for $\phi > \phi_m^*$. According to the Daoud–Cotton theory,[43,59] we use the prediction that the radius of the micelles, and therefore also σ_{int}, shrinks following $\sigma_{int} \sim (\phi/\phi_m^*)^{-1/8}$ above the overlap volume fraction. This scaling behavior was experimentally confirmed by Laurati[10,25,37] for PEP–PEO star-like micelles with $N_{agg} = 63$, 67, and 136, where a sufficient number of samples above ϕ_m^* were measured. Finally, the refined σ_{int} has been used to obtain a correct estimation of the theoretical volume fraction ϕ_{TH}.[10,14,25,37] Here, we emphasize that N_z is independently and unambiguously known from experiment. For the most symmetric block-ratio $1 : 2$, which resembles compact hard spheres, the packing

fraction is equivalent to corresponding hard sphere volume fraction ($\phi_{TH} \cong \phi_{HS}$). In this case, the interaction length is manifested as the micellar diameter $\sigma_{int} = 2R_m$ but the effective potential is, accordingly, not the one given by eqn (1) but rather a hard-sphere interaction with diameter $d_{HS} \cong \sigma_{int}$.

3.3 Dynamics of soft colloids

The quantitative description of microscopic architecture, interactions and resulting structure, is used in the following to understand the meso- and macroscopic dynamics of soft colloids. In this regard some advanced rheological characterization[60,61] of the macroscopic flow properties is prerequisite. The results from rheology and dynamic light scattering measurements are reported in Fig. 4. With increasing ϕ, a
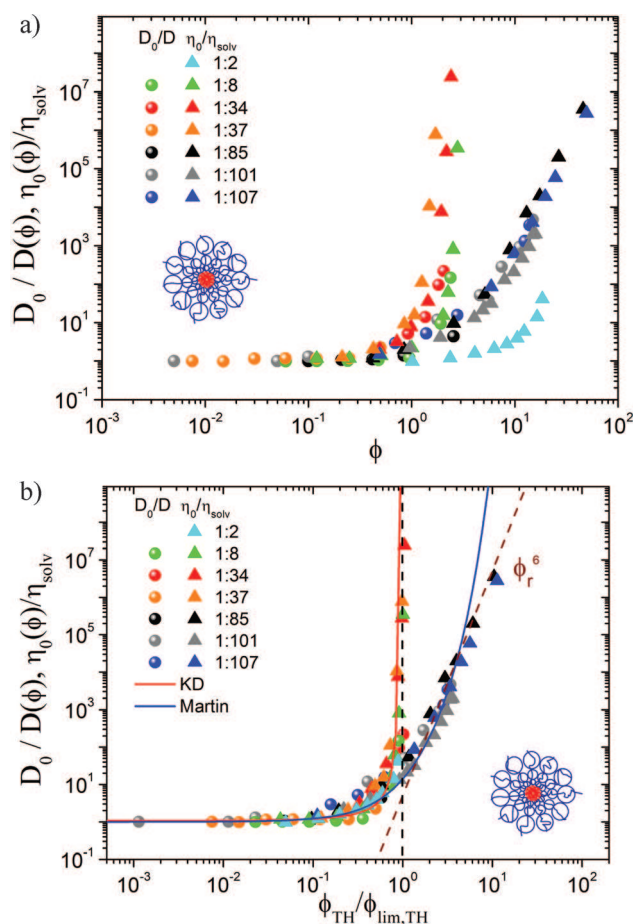

Fig. 4 Reduced viscosity $\eta_0(\phi)/\eta_{solv}$ (solid upward triangles) and self-diffusion coefficient $D_0/D(\phi)$ (solid circles) for different block-ratios, as function of (a) polymer volume fraction and (b) reduced theoretical volume fraction $\phi_r = \phi_{TH}/\phi_{lim,TH}$. For the highly asymmetric block ratios ($1 : 85$, $1 : 101$ and $1 : 107$) the overlap volume fraction from SANS has been used to evaluate $\phi_{lim,TH}$, whereas for the symmetric block ratios ($1 : 2$, $1 : 8$, $1 : 34$ and $1 : 37$) we employed values from DLS and rheology. The vertical dashed line represents ϕ_r^0 and the sloped dashed line a $\sim\phi_r^6$ power law dependence for the symmetric and asymmetric block ratios, respectively. Inset in (a) and (b): schematic illustration of star-like block-copolymer micelles.

divergence of the zero-shear viscosity η_0 is observed for block ratios $1:2$, $1:8$, $1:34$ and $1:37$, whereas for the most asymmetric block ratios $1:85$, $1:101$ and $1:107$ data follow a power law increase, as illustrated in Fig. 4(a), where the viscosity has been normalized by the solvent viscosity η_{solv}. It provides a generalized description of the reduced viscosity, which facilitates a precise comparison of macroscopic flow properties for micelles with varying softness. From dynamic light scattering (DLS) measurements, the underlying slow diffusive mode was identified as the self diffusion of the micelles.[31] Then, it is also expected that the inverse of the self-diffusion coefficient $D(\phi)$ behaves in a similar way to $\eta_0(\phi)$ i.e., $D(\phi) \propto 1/\eta_0(\phi)$. As can be seen in Fig. 4(a), indeed the reduced quantity $D_0/D(\phi)$, where $D_0 = D(\phi = 0)$, nicely fall on top of the rheology data $\eta_0(\phi)/\eta_{solv}$ for all block ratios and exhibits either the same divergence at a critical volume fraction ϕ_c or the same power law increase.

This allows us to bring the results from rheology and DLS for all different block-ratios plotted together to obtain generic master curves, as shown in Fig. 4(b). Clearly all data from the seven block ratios under investigation and shown in Fig. 4(a) merge into two classes. A divergence of reduced viscosity $\eta_0(\phi)/\eta_{solv}$ and of the inverse of the self-diffusion coefficient $D_0/D(\phi)$ is clearly seen for the more symmetric block-ratio, where the polymer volume fraction ϕ has been recast onto the effective reduced packing fraction $\phi_r = \phi_{TH}/\phi_{lim,TH}$ obtained from SANS. The limiting volume fraction $\phi_{lim,TH}$ is obtained from fitting to the Krieger–Dogerty (KD) model[62] for the symmetric block ratios. For the most asymmetric block-ratios, showing no clear divergence, the data can be collapsed again. Here, we used the Martin relation[63,64] (see ESI†). Our data rather seems to follow a power law, $\sim\phi_r^6$ at higher volume fractions. For these highly asymmetric mixtures, we identified $\phi_{lim,TH}$ with the overlap micelle packing fraction ϕ_m^* to express the results on the same abscissa as for the more symmetric ones.

4. Discussion

As observed from experimental and theoretical results, the variation of the block ratio controls in a well defined manner both the aggregation number (N_{agg}) and the morphology of the micelles, from ultrasoft star-like to hard sphere-like architecture, as independently determined by SANS in dilute solution, see Fig. 2. Concomitantly it also governs the coarse-grained, effective micelle–micelle interaction in concentrated solutions, see Fig. 3, as demonstrated by combining SANS and liquid state theory. This in turn crucially affects the macroscopic flow properties at higher concentrations, as well as the corresponding mesoscopic micellar dynamics, whose dependence on the volume fraction was investigated in detail by rheology and DLS, respectively. The master curves combining results from both dynamic methods clearly show the existence of two classes of dynamical behavior depending on the colloidal softness, as shown in Fig. 4(b). Similar features were found for regular star polymers but in a rather limited range of
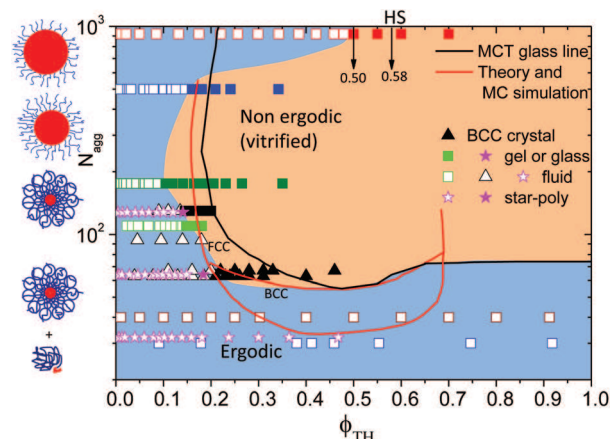

Fig. 5 Generalized experimental phase diagram for star-like soft colloids as a function of the aggregation number (N_{agg}) and the (theoretical) packing fraction (ϕ_{TH}). All the open symbols represent fluid or ergodic phase. Solid squares and stars represent the gel/glass[32] phase (non-ergodic), whereas the solid triangles represent the BCC-crystal-line[10,25] phase. Solid lines indicate the theoretical equilibrium phase diagram,[14,65] and the MCT ideal glass line.[32] Here the stars represent comparison with real polybutadiene star-polymers as calculated from Vlassopoulos et al.[31,66] Data marked by black symbols are taken from Laurati et al.[10,25] whereas the colored ones are new results. Side sketches: schematic representation of the micelles and unimers with change in N_{agg}.

functionalities/aggregation numbers,[31] which again emphasizes the versatility of block copolymer micelles as easy-to-establish tunable soft colloids.

All these aspects are finally brought together by the generalized dynamic phase diagram for soft colloids illustrated in Fig. 5, which bears the signature of so called structure–property–relationship (SPR), bringing quantitatively together microscopic molecular structure and macroscopic flow properties. In Fig. 5, data obtained in this work for the new PBO–PEO system, covering two orders of magnitude in N_{agg}, are shown together with those of PEP–PEO diblock copolymer micelles investigated by Laurati et al.[10,25,37] and with real polybutadiene star-polymers from Vlassopoulos et al.[31,66] All are quantitatively compared with the theoretical phase diagram,[14,65] including the MCT ideal glass line,[32] without the introduction of any adjustable parameter.

A comprehensive agreement is observed between theory and experiment in Fig. 5, in particular with respect to the location of the liquid-solid phase boundary. In agreement with the theoretical predictions, and to the best of our knowledge for the first time, we find a clear reentrance of the liquid–glass transition at fixed ϕ_{TH} as a function of the functionality: indeed, the star-like samples at constant ϕ_{TH} within the region $0.1 \lesssim \phi_{TH} \lesssim 0.2$ are ergodic for low aggregation numbers, they glassify for intermediate ones and then they become fluid again at even higher ones. For the most symmetric block copolymer, for which $N_{agg} = 920 \pm 20$, the ergodic-to-nonergodic transition occurs at a volume fraction very close to the known

value for hard spheres,[67,68] *i.e.*, $\phi_{HS}^{(g)} \simeq 0.58$. This finding is in full agreement with the single-particle, form factor analysis shown in Fig. 3, in which it was found that this system is not described by a starlike corona but rather by a compact, hard-sphere-like shape. The small discrepancy between the packing fraction of the glass transition for the $m:n = 1:2$-system and the hard-sphere one, $\phi_{TH}^{(g)} < \phi_{HS}^{(g)} = 0.58$, can be attributed to additional repulsive interactions from the solvophilic chains, which act to bring about an effective hard-sphere diameter that slightly exceeds the particle size. This would be a typical behavior for soft colloids, as similar features have also been reported by Mattsson *et al.*[68] for microgel suspensions. Finally, the significant difference in Fig. 5 between the location of the glass line for the starlike interaction and the experimental result for the highest aggregation number can be easily understood: the theoretical result is based on the assumption that the particles still have a starlike conformation, which is not the case for the experimental system at hand, since the symmetric nature of the underlying block copolymer renders the height of the sovophilic corona too short to give the latter the characteristics of the spherical Daoud–Cotton brush.

We did not find formation of ordered crystals for the systems at hand. A possible explanation for the ability of the PEP–PEO system[10,25] to crystallize into a BCC structure for aggregation number $N_{agg} < 70$ in contrast to the present PBO–PEO system, which tends to form an amorphous solid, might be due to the copolymer exchange between micelles (living micelles), as measured in time-resolved SANS measurements by Lund *et al.*[69,70] Since Laurati *et al.*[10,25,37] varied N_{agg} by changing the composition of the solvent, *i.e.*, the interfacial tension on addition of DMF (*N,N*-dimethylformamide), the packing of micelles in ordered structures could be facilitated with increasing volume fraction, which has been observed also for other living micellar systems.[8,9] Although the PEP–PEO system apparently forms frozen micelles over the whole range of polymer volume fractions at room temperature, slow exchange dynamics could not be totally excluded for high amounts of DMF. However no FCC crystalline structure was observed by Laurati *et al.*, at least not in a time period of 2 weeks after sample preparations. For our PBO–PEO micellar systems perfectly frozen micelles were formed for higher aggregation number, *i.e.*, $100 \lesssim N_{agg} \lesssim 900$, since we just changed the PBO : PEO block-ratio and kept the solvent composition fixed. Here no crystalline phase was detected, as no Bragg peaks were observed in SANS measurements. We identified an amorphous glassy state for $\phi > \phi_m^*$, as verified from extensive investigation of the micellar dynamics using rheology and DLS. It could be speculated that the absence of significant block copolymer exchange between micelles hampers the ordering into the crystalline phase as recently discussed by Nicolai and co-workers.[71] Moreover, the observation of crystalline phases is extremely sensitive to polydispersity which is unavoidable in colloidal suspensions. Such disordered-amorphous, dynamically arrested states for $\phi > \phi_m^*$ has been also reported for PB stars[72,73] when $N_{agg} > 70$. The dynamical arrest was explained in terms of cluster formation when the arms in

the outermost blobs of the particles start to overlap. For large chains, the segment density in the corona causes sufficient geometric confinement that can strongly suppress the chain dynamics, leading to the formation of clusters. Even a small number of clusters could induce a macroscopically arrested state.[73] These clusters on approaching the overlap volume fraction could finally lead to dynamical arrest of the system at smaller values of the packing fraction ϕ_{TH} than predicted by MCT.[32] Whereas for $\phi \gtrsim \phi_m^*$ the cage effect suppresses the dynamics significantly, the clustering could be manifested as an "effective" polydispersity in the sample,[74] which suppresses the underlying crystalline phases.

The general effect of the polydispersity is to destroy order, *i.e.*, to suppress crystallization. In case of binary mixtures of hard spheres and also in other complex fluids where the polydispersity has been deliberately introduced into the system, both from experiments[75] and simulations[76–79] it has been observed that for hard-spheres 5–10% polydispersity configures the terminal value, defined as the maximum polydispersity above which the system exhibits an amorphous glassy state, without showing any crystalline phase. It is to be noted that block-copolymers inherit some polydispersity in molecular weights from their synthesis mechanism (although anionic polymerization is known to give the best possible monodisperse polymers), which could effectively results in size polydispersity. In such case, polydispersity in can be defined as[33] $p = 1 - M_w/M_n$, which could then range between 2% $\lesssim p \lesssim$ 10% for different block-ratios (see Table 1). According to some recent studies by Stiakakis *et al.*[80] on crystallization of multi-arm stars by multi-speckle dynamic light scattering (MSDLS) and SANS, slow aging of the initially frustrated glassy state can leads to star crystallization. This could be one of the possible reason that we did not observe crystallization within an experimental time window of 2–3 weeks.

5. Conclusions

In the present work, we introduced a new block copolymer system which enables us to investigate a broad range of micellar aggregation numbers $10 \leq N_{agg} \leq 1000$ and concentrations $0.1 \leq \phi_{TH}/\phi_{TH}^* \leq 10$ of soft colloids using the same well-defined model. We interpret rheological and dynamic light scattering (DLS) data in terms of recently developed experimental and theoretical approaches that quantitatively describe microscopic structure as observed by complimentary small angle neutron scattering (SANS) experiments. This finally enabled us to derive the dynamic phase diagram of soft colloids showing convincing agreement between experiment and theory. In the following, we elaborate in detail some particular points following concerning our results.

In the first place, the micellar morphology, *i.e.*, the microscopic structure of the individual soft colloid as seen in the form factor $P(Q)$ determined by SANS, can be smoothly varied from hard sphere-like to ultrasoft star-like by adjusting the block-ratio $m:n$ from (nearly) symmetric to highly asymmetric,

i.e. 1 : 2, 1 : 8, 1 : 34, 1 : 37, 1 : 85, 1 : 89, 1 : 101 and 1 : 107. Form factor analysis in dilute solution provides independently the basic parameters N_{agg} and R_m necessary for the subsequent structure factor analysis in concentrated solution. In this direction, we confirmed and extended for a broad range of micellar morphologies a way to calculate the crucial interaction length σ_{int} from R_m (SANS) and R_h (DLS). The corresponding value of σ_{int} has been verified by the procedure of elaborate comparison between theory and SANS experiments. It is to be noted that no adjustable parameter is required, hence a satisfactory model of structure factor and the corresponding SANS intensities was obtained over a broad range of volume fraction for several block ratios. In this way, the obtained value of the interaction length σ_{int} has been identified as the one and only natural length scale governing both structure and dynamics of soft colloids. Its concentration dependence follows a power-law $\phi^{-1/8}$ for $\phi > \phi_m^*$ only, which has been confirmed and also employed to express the block copolymer volume fraction ϕ into micellar ϕ_m and theoretical ϕ_{TH} packing fractions. We conclusively verified the validity of the coarse-grained potential given by eqn (1) in accurately describing the (mesoscopic) effective interaction between star-like, polymer-based soft colloids.

From the experimental scattering intensity $I(Q)$, no crystalline phases have been observed over a broad range of aggregation number ($50 \lesssim N_{agg} \lesssim 900$); rather the system shows amorphous glassy behavior for $\phi > \phi_m^*$, which lies close to the MCT glass line as predicted by theory and simulations in the phase diagram. We observe for the first time a clear reentrance of the glass transition recovering the equivalent hard-sphere volume fraction at the highest aggregation number, $N_{agg} \simeq 10^3$. From the dynamical point of view, it has been verified that both the shear viscosity η_0 and the inverse of the self diffusion coefficient D_S behave in the same way around the overlap volume fraction ϕ_m^* of the micelles, apparently showing a strong correlation between mesoscopic diffusion and macroscopic viscosity, irrespective of softness of the colloids.

Finally, all the information related to both the statics and dynamics of the considered soft colloids has been brought together in an experimental dynamic phase diagram which was compared with the theoretical one. Again, the packing fraction ϕ_{TH} based on σ_{int} as the relevant length scale, was shown to be the appropriate reduction parameter for the concentration dependence, allowing a generic description of the macroscopic viscosity $\eta_0(\phi)$, the mesoscopic diffusivity dynamics $D(\phi)$ and microscopic structure $S(Q)$, and comparison of these properties for particles with varying softness. The excellent agreement between our new experimental systems with different but already established model systems[10,27] shows the relevance of block copolymer micelles as a clever realization of soft colloids and the general validity of the coarse-graining approximation for describing structural, dynamical and phase features of dense, soft colloid suspensions, which understanding could provide guidance in the rational design of materials for targeted applications.

References

1 D. Vlassopoulos and M. Cloitre, *Soft Matter*, 2012, **8**, 4010.
2 D. Vlassopoulos and M. Cloitre, *Curr. Opin. Colloid Interface Sci.*, 2014, **19**, 561–574.
3 M. Ballauff and C. N. Likos, *Angew. Chem., Int. Ed.*, 2004, **43**, 2998.
4 H. M. Wyss, K. Miyazaki, J. Mattsson, Z. Hu, D. R. Reichman and D. A. Weitz, *Phys. Rev. Lett.*, 2007, **98**, 238303.
5 *Microgel Suspensions - Fundamentals and Applications*, ed. A. Fernandez-Nieves, H. Wyss, J. Mattson and D. A. Weitz, Wiley-VCH, Weinheim, 2011.
6 T. B. Martin, P. M. Dodd and A. Jayaraman, *Phys. Rev. Lett.*, 2013, **110**, 018301.
7 I. W. Hamley, *The Physics of Block Copolymers*, Oxford University Press, Oxford, UK, 1998.
8 J. Bang and T. P. Lodge, *Phys. Rev. Lett.*, 2004, **93**, 245701.
9 T. Nicolai, F. Lafleche and A. Gibaud, *Macromolecules*, 2004, **37**, 8066.
10 M. Laurati, J. Stellbrink, R. Lund, L. Willner, D. Richter and E. Zaccarelli, *Phys. Rev. Lett.*, 2005, **94**, 195504.
11 J. Stellbrink, J. Allgaier, M. Monkenbusch, D. Richter, A. Lang, C. N. Likos, M. Watzlawek, H. Löwen, G. Ehlers and P. Schleger, *Prog. Colloid Polym. Sci.*, 2000, **115**, 88.
12 S. A. Rogers, D. Vlassopoulos and P. T. Callaghan, *Phys. Rev. Lett.*, 2008, **100**, 128304.
13 B. M. Erwin, D. Vlassopoulos and M. Cloitre, *J. Rheol.*, 2010, **54**, 915.
14 C. N. Likos, *Phys. Rep.*, 2001, **348**, 267.
15 R. Lund, *PhD Thesis*, University of Münster, 2004.
16 T. A. Witten, P. A. Pincus and M. E. Cates, *Macromolecules*, 1986, **19**, 2509.
17 C. N. Likos, H. Löwen, M. Watzlawek, B. Abbas, O. Jucknischke, J. Allgaier and D. Richter, *Phys. Rev. Lett.*, 1998, **80**, 4450.
18 H. Löwen, *Phys. Rep.*, 1994, **237**, 249.
19 J. P. Hansen and I. R. McDonald, *Theory of simple liquids*, Academic Press, London, 2006.

20 M. Ballauff and O. Borisov, *Curr. Opin. Colloid Interface Sci.*, 2006, **11**, 316.

21 M. Ballauff, *Prog. Polym. Sci.*, 2007, **32**, 1135.

22 F. Lo Verso, L. Yelash, S. A. Egorov and K. Binder, *J. Chem. Phys.*, 2011, **135**, 214902.

23 F. Lo Verso, S. A. Egorov and K. Binder, *Macromolecules*, 2012, **45**, 8892.

24 Y. Lu, M. Ballauff and A. Wittemann, *Polym. Sci. Comprehensive Ref.*, 2012, **6**, 265.

25 M. Laurati, J. Stellbrink, R. Lund, L. Willner, E. Zaccarelli and D. Richter, *Phys. Rev. E: Stat. Phys., Plasmas, Fluids, Relat. Interdiscip. Top.*, 2007, **76**, 041503.

26 M. Camargo and C. N. Likos, *Phys. Rev. Lett.*, 2010, **104**, 078301.

27 B. Lonetti, M. Camargo, J. Stellbrink, C. N. Likos, E. Zaccarelli, L. Willner, P. Lindner and D. Richter, *Phys. Rev. Lett.*, 2011, **106**, 228301.

28 L. Mohan, R. T. Bonnecaze and M. Cloitre, *Phys. Rev. Lett.*, 2013, **111**, 268301.

29 L. Gentile, M. A. Behrens, S. Balog, K. Mortensen, G. A. Ranieri and U. Olsson, *J. Phys. Chem. B*, 2014, **118**, 3622–3629.

30 L. Gentile, L. Coppola, S. Balog, K. Mortensen, G. A. Ranieri and U. Olsson, *ChemPhysChem*, 2015, DOI: 10.1002/cphc.201500237.

31 D. Vlassopoulos, G. Fytas, T. Pakula and J. Roovers, *J. Phys.: Condens. Matter*, 2001, **13**, R855–R876.

32 G. Foffi, F. Sciortino, P. Tartaglia, E. Zaccarelli, F. Lo Verso, L. Reatto, K. A. Dawson and C. N. Likos, *Phys. Rev. Lett.*, 2003, **90**, 238301.

33 M. Rubinstein and R. Colby, *Polymer Physics*, Oxford University Press, Oxford, 2003.

34 J. Allgaier, S. Willbold and T. Chang, *Macromolecules*, 2007, **40**, 518.

35 M. Ströbl, *Diploma Thesis*, University of Regensburg, 2008.

36 T. Nicolai, *Soft Matter*, 2010, **6**, 3111.

37 M. Laurati, *PhD Thesis*, University of Münster, 2005.

38 S. Abbas and T. P. Lodge, *Phys. Rev. Lett.*, 2007, **99**, 137802.

39 S. Gupta, *PhD Thesis*, University of Münster, 2012.

40 V. Pippich, *QtiKWS10, DAN-light*, 2011, http://www.qtikws.de.

41 D. Richard, M. Ferrand and G. J. Kearley, *LAMP*, 2011, https://www.ill.eu/instruments-support/computing-for-science/cs-software/all-software/lamp/.

42 G. Petekidis, D. Vlassopoulos and P. N. Pusey, *J. Phys.: Condens. Matter*, 2004, **16**, S3955–S3963.

43 M. Daoud and J. P. Cotton, *J. Phys.*, 1982, **43**, 531.

44 L. Willner, A. Poppe, J. Allgaieri, M. Monkenbusch, P. Lindner and D. Richter, *Europhys. Lett.*, 2000, **51**, 628.

45 C. Mayer and C. N. Likos, *Macromolecules*, 2007, **40**, 196.

46 F. Randisi and A. Pelissetto, *J. Chem. Phys.*, 2013, **139**, 154902.

47 A. Jusufi, J. Dzubiella, C. N. Likos, C. Ferber and H. Löwen, *J. Phys.: Condens. Matter*, 2001, **13**, 6177.

48 R. L. C. Vink, A. Jusufi, J. Dzubiella and C. N. Likos, *Phys. Rev. E: Stat. Phys., Plasmas, Fluids, Relat. Interdiscip. Top.*, 2005, **72**, 030401(R).

49 P. Linder, *Neutrons, X-rays, and Light: Scattering methods applied to soft condensed matter*, North-Holland Delta Series, Elsevier, Amsterdam, 2002.

50 C. Svaneborg and J. S. Pedersen, *Phys. Rev. E: Stat. Phys., Plasmas, Fluids, Relat. Interdisc. Top.*, 2001, **64**, 010802.

51 J. S. Pedersen, C. Svaneborg, K. Almdal, I. W. Hamley and R. N. Young, *Macromolecules*, 2003, **36**, 416–433.

52 R. Lund, V. Pipich, L. Willner, A. Radulescu, J. Colmenero and D. Richter, *Soft Matter*, 2011, **7**, 1491–1500.

53 R. Lund, L. Willner, M. Monkenbusch, P. Panine, T. Narayanan, J. Colmenero and D. Richter, *Phys. Rev. Lett.*, 2009, **102**, 188301.

54 M. Fuchs and M. Müller, *Phys. Rev. E: Stat. Phys., Plasmas, Fluids, Relat. Interdiscip. Top.*, 1999, **60**, 1921.

55 P. G. de Gennes, *Scaling Concepts in Polymer Physics*, Cornell University Press, Ithaca, NY, 1979.

56 G. Beaucage, *J. Appl. Crystallogr.*, 1995, **28**, 717.

57 G. Beaucage, *J. Appl. Crystallogr.*, 1996, **29**, 134.

58 J. S. Pedersen, A. Posselt and K. Mortensen, *J. Appl. Crystallogr.*, 1990, **23**, 321.

59 D. Richter, O. Jucknischke, L. Willner, L. J. Fetters, M. Lin, J. S. Huang, J. Roovers, C. Toporowski and L. L. Zhou, *J. Phys. IV*, 1993, **3**, 3.

60 S. Gupta, S. K. Kundu, J. Stellbrink, L. Willner, J. Allgaier and D. Richter, *J. Phys.: Condens. Matter*, 2012, **24**, 464102.

61 S. Kundu, S. Gupta, J. Stellbrink, L. Willner and D. Richter, *Eur. Phys. J. special Topics*, 2013, **222**, 2757–2772.

62 I. M. Krieger and T. J. Dougherty, *Trans. Soc. Rheol.*, 1959, **3**, 137.

63 W. M. Macosko, *Rheology Principles, Measurements and Applications*, Wiley-VCH, New York, 1994.

64 A. Asteriadi, R. Sigel, D. Vlassopoulos, G. Meier, J. R. Dorgan and D. M. Knauss, *Macromolecules*, 2004, **37**, 1016.

65 M. Watzlawek, C. N. Likos and H. Löwen, *Phys. Rev. Lett.*, 1999, **82**, 5289.

66 D. Vlassopoulos, G. Fytas, S. Pispas and N. Hadjichristidis, *Physica B*, 2001, **296**, 184–189.

67 W. Van Megen and P. N. Pusey, *Phys. Rev. A*, 1991, **43**, 5429.

68 J. Mattsson, H. M. Wyss, A. Fernandez-Nieves, K. Miyazaki, Z. B. Hu, D. R. Reichman and D. A. Weitz, *Nature*, 2009, **462**, 83.

69 R. Lund, L. Willner, J. Stellbrink, P. Lindner and D. Richter, *Phys. Rev. Lett.*, 2006, **96**, 068302.

70 R. Lund, L. Willner, D. Richter and E. E. Dormidontova, *Macromolecules*, 2006, **39**, 4566.

71 F. Puaud, T. Nicolai, E. Nicol, L. Benyahia and G. Brotons, *Phys. Rev. Lett.*, 2013, **110**, 028302.

72 J. Roovers, *Macromolecules*, 1994, **27**, 5359.

73 M. Kapnistos, D. Vlassopoulos, G. Fytas, K. Mortensen, G. Fleischer and J. Roovers, *Phys. Rev. Lett.*, 2000, **85**, 4072.

74 F. Sciortino, S. Mossa, E. Zaccarelli and P. Tartaglia, *Phys. Rev. Lett.*, 2004, **93**, 055701.

75 P. Bartlett and P. B. Warren, *Phys. Rev. Lett.*, 1999, **82**, 1979.

76 W. Kob and H. C. Andersen, *Phys. Rev. Lett.*, 1994, **73**, 1376.

77 R. M. L. Evans, D. J. Fairhurst and W. C. K. Poon, *Phys. Rev. Lett.*, 1998, **81**, 1326.

78 D. A. Kofke and P. G. Bolhuis, *Phys. Rev. E: Stat. Phys., Plasmas, Fluids, Relat. Interdiscip. Top.*, 1999, **59**, 618.

79 S. R. Williams, I. K. Snook and W. van Megen, *Phys. Rev. E: Stat. Phys., Plasmas, Fluids, Relat. Interdiscip. Top.*, 2001, **64**, 021506.

80 E. Stiakakis, A. Wilk, J. Kohlbrecher, D. Vlassopoulos and G. Petekidis, *Phys. Rev. E: Stat. Phys., Plasmas, Fluids, Relat. Interdiscip. Top.*, 2010, **81**, 020402(R).